

Risk Assessment and Mitigation in Local Path Planning for Autonomous Vehicles With LSTM Based Predictive Model

Hong Wang^{ID}, Bing Lu^{ID}, Jun Li, Teng Liu^{ID}, *Member, IEEE*, Yang Xing^{ID}, Chen Lv^{ID}, *Senior Member, IEEE*, Dongpu Cao^{ID}, Jingxuan Li^{ID}, Jinwei Zhang, and Ehsan Hashemi^{ID}, *Member, IEEE*

Abstract—Accurate trajectory prediction of surrounding vehicles enables lower risk path planning in advance for autonomous vehicles, thus promising the safety of automated driving. A low-risk and high-efficiency path planning approach is proposed for autonomous driving based on the high-performance and practical trajectory prediction method. A long short-term memory (LSTM) network is trained and tested using the highD dataset, and the validated LSTM is used to predict the trajectories of surrounding vehicles combining the information extracted from vehicle-to-vehicle (V2V) technology. A risk assessment and mitigation-based local path planning algorithm is proposed according to the information of predicted trajectories of surrounding vehicles. Two driving scenarios are extracted and reconstructed from the highD dataset for validation and evaluation, i.e., an active lane-change scenario and a longitudinal collision-avoidance scenario. The results illustrate that the risk is mitigated and the driving efficiency is improved with the proposed path planning algorithm comparing to the constant-velocity prediction and the prediction method of the nonlinear input–output (NIO) network, especially when the velocity and trajectory with sudden changes.

Note to Practitioners—This article was motivated by the problem of promising the safety decision-making and path planning through accurate environment prediction. There are two main parts included in this article. First, this article proposed one prag-

Manuscript received 10 February 2021; accepted 18 April 2021. Date of publication 25 May 2021; date of current version 13 October 2022. This article was recommended for publication by Editor H. Gao upon evaluation of the reviewers' comments. This work was supported in part by the National Science Foundation of China under Project 52072215 and Project U1964203 and in part by the National Key Research and Development Program of China under Grant 2020YFB1600303. (Corresponding authors: Bing Lu; Teng Liu.)

Hong Wang and Jun Li are with the Tsinghua Intelligent Vehicle Design and Safety Research Institute, Tsinghua University, Beijing 100084, China (e-mail: hong_wang@tsinghua.edu.cn; lijun1958@tsinghua.edu.cn).

Bing Lu is with the Beijing Institute of Technology, Beijing 100811, China, and also with the Department of Mechanical and Mechatronics Engineering, University of Waterloo, Waterloo, ON N2L 3G1, Canada (e-mail: lubingev@sina.com).

Teng Liu, Dongpu Cao, Jinwei Zhang, and Ehsan Hashemi are with the Department of Mechanical and Mechatronics Engineering, Waterloo University, Waterloo, ON N2L 3G1, Canada (e-mail: tengliu17@gmail.com; dongpu.cao@uwaterloo.ca; jinwei.zhang@uwaterloo.ca; ehashemi@uwaterloo.ca).

Yang Xing and Chen Lv are with the School of Mechanical and Aerospace Engineering, Nanyang Technological University, Singapore (e-mail: yxing_edu@163.com; lyuchen@ntu.edu.sg).

Jingxuan Li is with the College of Energy and Power Engineering, Nanjing University of Aeronautics and Astronautics, Nanjing 210016, China (e-mail: 269199917@qq.com).

Color versions of one or more figures in this article are available at <https://doi.org/10.1109/TASE.2021.3075773>.

Digital Object Identifier 10.1109/TASE.2021.3075773

matic approach to predict the environment movement correctly based on the long short-term memory (LSTM) approach. The prediction performance of LSTM was compared with nonlinear input–output (NIO). The results showed that the LSTM approach has a significant advantage in motivation prediction of the surrounded vehicles during path planning. The second part of this article is to make the decision and realize local path planning based on the risk assessment. The potential field-based approach is implemented on the risk assessment based on these accurate predictions. Some primary results demonstrate that the decision-making algorithm performs better under the accurate prediction model. The results also show that the safety and driving efficiency of the ego vehicle were improved by tracking the trajectory, which was planned based on the risk assessment. The only concern for the real-time application is the computation time; in future, we will figure it out how to further reduce the computation time.

Index Terms—HighD dataset, local path planning, long short-term memory (LSTM), model predictive control (MPC), risk assessment, risk mitigation.

NOMENCLATURE

Parameters	Definition	Unit
a_i	shape coefficient	[unitless]
$\Delta u_{a,i}$	longitudinal approaching velocity	[m/s]
a_n	maximum comfort deceleration	[m/s ²]
dX	differential of longitudinal distance	[m]
$Y_{s,i}$	lateral safe distance	[m]
X_o	minimum longitudinal distance	[m]
T_0	safe time gap	[s]
$u_{o,i}$	velocity of obstacle	[m/s]
v_x	longitudinal velocity	[m/s]
ω	yaw rate	[rad/s]
Y	lateral position	[m]
m	vehicle mass	[kg]
$F_{y,f}$	lateral force of front tire	[N]
L_f	front wheelbase	[m]
I_z	vehicle rotation inertia	[kg·m ²]
C_r	corner-stiffness of rear tire	[N/deg]
α_r	sideslip angle of rear tire	[deg]
v_x^{\max}	velocity limitation	[m/s]
$F_{y,\max}$	maximum lateral tire force	[N]
δ_{\max}	maximum steering limitation	[rad]
b_i	intensity coefficient	[unitless]
$\Delta v_{a,i}$	lateral approaching velocity	[m/s]

θ	heading angle	[deg]
dY	differential of lateral distance	[m]
$X_{s,i}$	longitudinal safe distance	[m]
Y_o	minimum lateral distance	[m]
u	velocity of ego vehicle	[m/s]
D_a	minimum distance from road boundary	[m]
v_y	lateral velocity	[m/s]
X	longitudinal position	[m]
φ	heading angle	[rad]
F_x	longitudinal tire force	[N]
$F_{y,r}$	lateral force of rear tire	[N]
L_r	rear wheelbase	[m]
C_f	corner-stiffness of front tire	[N/deg]
α_f	sideslip angle of front tire	[deg]
δ	steering angle	[rad]
$F_{x,\max}$	maximum longitudinal tire force	[N]
μ	road adhesion coefficient	[unitless]
δ_{\min}	minimum steering limitation	[rad]

I. INTRODUCTION

A. Motivation

WITH the promise of improving traffic safety, the technologies of autonomous vehicles (AVs) were developed rapidly. However, there are AVs' accidents happened, especially several fatal accidents. For instance, there was one Uber test self-driving vehicle killed a woman in Temple, AZ, USA, in 2018 [1]. This incident in Temple was not the first time Uber's self-driving cars involved in a crash. Between September 2016 and March 2018, Uber's AVs were involved in 37 crashes and incidents [2]. Tesla equipped with autopilot also had several fatally crashes in the past three years [3]. Since the safety is always the first consideration from academia to manufacturers, it must be improved and proofed before the mass production of AVs [4]. To help improve both the cognitive ability and safety of AVs, the uncertainty analysis-based situational assessment is required and challenging [5]. Three typical safety problems are facing in current AVs: functional safety, the safety of the intended functionality (SOTIF), and cybersecurity [6]. SOTIF is caused by the system limitation or the foreseeable misuse. Current technologies, such as perception, path planning, decision-making, and actuation, still have limitations, especially when confronting complex driving scenarios. These kinds of issues are within the scope of SOTIF. Among these three safety challenges, the SOTIF is the biggest challenge for academia research and AVs application.

The path planning technology as one of the key technologies, which could directly impact the driving safety [7], has been widely developed. The heuristic path planning approaches, including A* [8], Dijkstra [9], and rapidly exploring random tree (RRT) [10], have the common feature that the paths generated from these methods are connected by a series of discrete waypoints, and these paths need further smoothing for practical application in AVs. Therefore, the optimization-based approaches, e.g., the artificial potential field (PF) approach [11], can be used to obtain the smooth and curvature continuous path. However, if the parameters of PF

functions are inappropriately configured or the obstacles are located with short distances, the route generated using PF is likely to fall into local minima, resulting in rough and unexpected routes [12]. Furthermore, learning-based approaches, e.g., reinforcement learning [13] and deep learning [14], are used to obtain the feasible and suboptimal trajectories based on the historical data. However, the feasible reward functions are usually hard to achieve, and the online application needs high cost on hardware to satisfy the real-time requirement. Moreover, many algorithms did not take the behaviors of surrounding vehicles and road boundaries into consideration, and the damage risks need to be assessed for ensuring the driving safety. To ensure the safety of AVs path planning, the AVs should have a better understanding of the surrounding environment, such as surrounding vehicles, pedestrians, and animals [15], if applicable. Therefore, a risk assessment and mitigation-based local path planning approach has been proposed by considering the situations of surrounding environment. With the accurate predictions of the surrounding obstacles, the AVs could make safer and more socially compliant decisions in advance resulting in guaranteeing the driving safety without losing too much comfort or being too conservative during the path planning and tracking [16].

As for the part of velocity/trajectory prediction, many algorithms have been researched and implemented on autonomous driving in the past decades. The methodologies can be classified into a long-term and a short-term method [17]. The long-term velocity/trajectory predictions are more trend-oriented, such as the driving cycle construction based on Monte Carlo [18], Markov Chain [19], data-driven autoregressive integrated moving average (ARIMA) [20], and dynamic tensor [21]. The short-term predictions are more state-oriented, such as state prediction based on unscented Kalman Filter [22], interactive multiple models [23], Bayesian Filter [24], and Gaussian Process [25]. Meanwhile, with the development of computer science, learning-based algorithms are developed for both long- [26] and short-term prediction [27]. With the capability of storing historical information of the extended time intervals according to feedback connection-nodes, the recurrent neural network (RNN) can be trained and applied as a predictor [28]. However, the gradient vanishing problem of the conventional RNN limited the application and development. The long short-term memory (LSTM) structure was developed to overcome the gradient vanish issue compared to the naively RNNs [29]. In recent years, the LSTM has been widely researched for trajectory/velocity prediction, e.g., in [30]–[32]. The feasible and robust issues of the LSTM prediction were proved as well in [33]. To this end, vehicle-to-vehicle (V2V) communication, over 5G new radio (NR) access or dedicated short-range communications (DSRC) using IEEE 802.11 technologies, can significantly enhance AVs safety by improving LSTM datasets. This connectivity helps improving the reliability of cooperative control and navigation tasks as well as fault diagnosis in vehicular networks through distributed state estimation and learning-aided control systems [34]–[37].

Since both the long-term trend and the short-term state of surrounding vehicles are important for driving safety during path planning of AVs, the predicted trajectories of surrounding

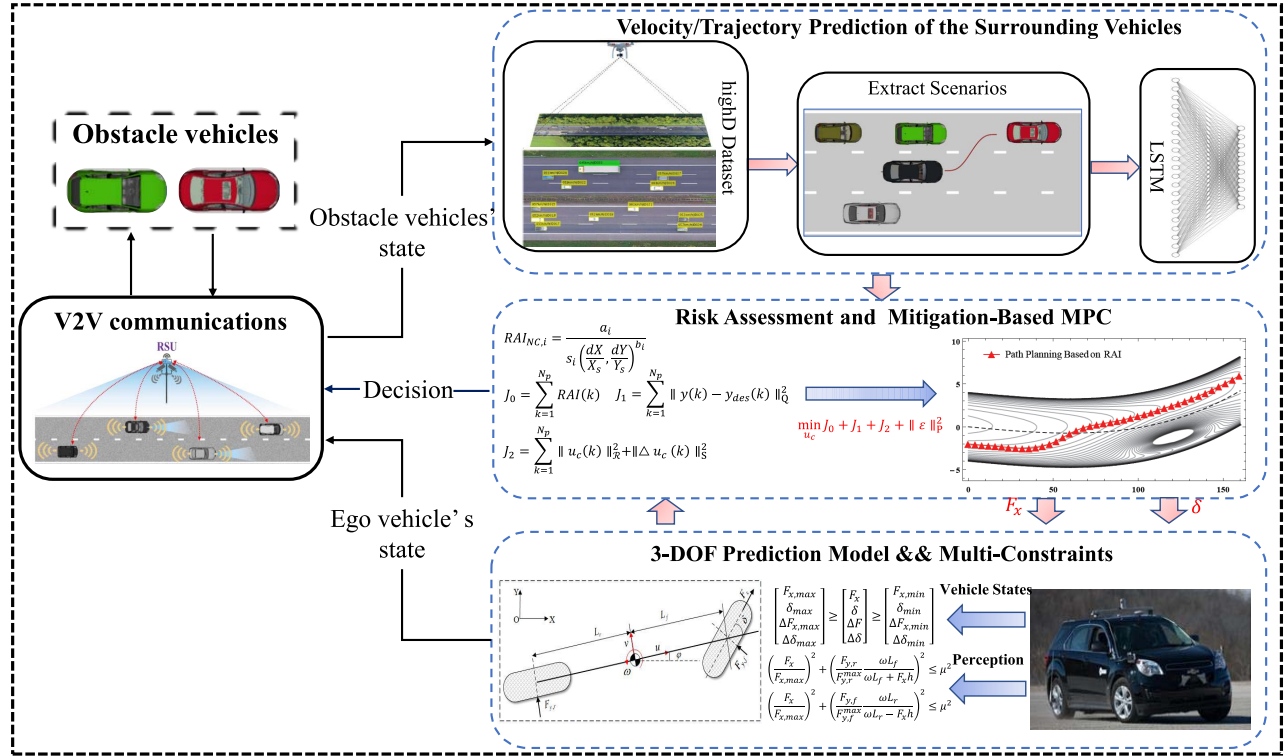


Fig. 1. Risk assessment and mitigation-based path planning for AVs with LSTM.

vehicles should include the long- and short-term features. The LSTM network is designed and trained for velocity prediction based on the highD dataset [38] in this article. Based on the predicted velocities of the surrounding vehicles, the driving risk is analyzed and predicted, and then, risk mitigation of local path planning algorithm was developed to promise the driving safety and efficiency.

B. Contributions

A risk assessment and mitigation-based local path planning approach is proposed to improve driving safety and efficiency by considering the accurate prediction of surrounding vehicles with the LSTM method. An LSTM network is established, trained, and tested for the velocity/trajjectory prediction of surrounding vehicles based on the highD dataset to overcome the bad effects of the uncertainty on interval distances, namely the driving safety. A risk assessment function is designed and calculated based on the trajectory prediction of LSTM for risk assessment. With the consideration of lowest risk, the local path planning is proposed for risk mitigation of autonomous driving.

C. Article Organization

This article works on path planning for AVs to mitigate crash severity during emergency situations. Section II presents the overall architecture for the risk assessment and mitigation-based path planning. Section III presents the control design for the crash mitigation path planning, including vehicle modeling, definition of crash severity factor, and PF adopted

to represent the environment. Section IV presents several case studies to verify the proposed control strategy for crash mitigation path planning and followed by the conclusion and future work in Section V.

II. FRAMEWORK OF THE RISK ASSESSMENT AND MITIGATION-BASED PATH PLANNING

Fig. 1 shows the path planning framework based on the risk assessment and mitigation for AVs in this article. The framework is composed of several stages, including the velocity predictions of the environment vehicles using LSTM, the risk assessment and mitigation-based path planning, and tracking using model predictive control (MPC) by considering the trajectories of surrounding vehicles. In Stage 1, the LSTM network is designed and trained to predict the velocities of surrounding vehicles based on the extracted data of highD dataset. In application, the predicted velocities of surrounding vehicles are obtained with the trained LSTM network based on the real-time and historical data collected by V2V technology. In Stage 2, the risk assessment is proceeded based on the predicted velocities by considering the approaching velocities and relative angles between ego vehicle and surrounding vehicles. Then, the local path planning algorithm is formulated as an optimization problem by considering the risk assessment item, tracking items, and slack variables. For brevity, this LSTM prediction model-based model predictive path planning and tracking control algorithm is named LSTM-MPC. Finally, the proposed LSTM-MPC is validated and evaluated by comparing to the traditional MPC (which adopts the constant-velocity prediction model) and

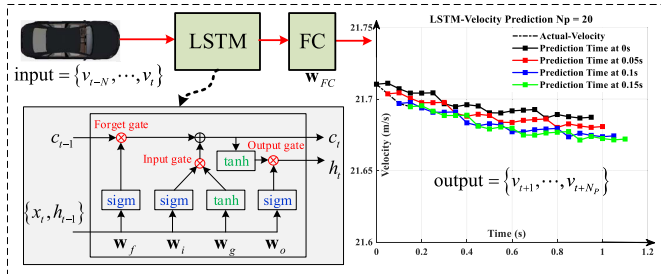


Fig. 2. Velocity prediction of the surrounding vehicles with LSTM.

TABLE I
LSTM EQUATIONS AND NETWORK STRUCTURE

LSTM equations:

$$\begin{aligned}
 \text{Input gate controller: } & i_t = \sigma(\mathbf{W}_{x,i}^T x_t + \mathbf{W}_{h,i}^T h_{t-1} + b_i) \\
 \text{Forget gate controller: } & f_t = \sigma(\mathbf{W}_{x,f}^T x_t + \mathbf{W}_{h,f}^T h_{t-1} + b_f) \\
 \text{Output gate controller: } & o_t = \sigma(\mathbf{W}_{x,o}^T x_t + \mathbf{W}_{h,o}^T h_{t-1} + b_o) \\
 \text{Activation function: } & g_t = \tanh(\mathbf{W}_{x,g}^T x_t + \mathbf{W}_{h,g}^T h_{t-1} + b_g) \\
 \text{Cell Memory: } & c_t = f_t \otimes c_{t-1} + i_t \otimes g_t \\
 \text{Output: } & y_t = h_t = o_t \otimes \tanh(c_t)
 \end{aligned}$$

Network structure in this paper:

$$\begin{aligned}
 \text{Layer Structure: } & 4 \times 1 \\
 \text{Input Layer: } & 1\text{-D}, x_t \in \mathbb{R} \\
 \text{LSTM Layer: } & 100 \text{ Units } h_{t-1} \in \mathbb{R}^{100 \times 1} \\
 (\mathbf{W}_{x,i}, \mathbf{W}_{x,f}, \mathbf{W}_{x,o}, \mathbf{W}_{g,i}) & \in \mathbb{R}^{100 \times 1} \\
 (\mathbf{W}_{h,i}, \mathbf{W}_{h,f}, \mathbf{W}_{h,o}, \mathbf{W}_{h,i}) & \in \mathbb{R}^{100 \times 100} \\
 \text{Fully connected layer: } & \mathbf{W}_{FC} \in \mathbb{R}^{100 \times 20} \\
 \text{Output Layer: } & \text{Regression}
 \end{aligned}$$

the nonlinear input–output (NIO)-based MPC in two driving scenarios extracted from the highD dataset.

III. LSTM-BASED PREDICTION MODEL

Since the path planning algorithm is extremely sensitive to the positions of surrounding obstacles, it is necessary to predict the trajectories of the surrounding obstacles in real-time [39]. Especially, the risk of obstacle avoidance will increase when the surrounding vehicles have sudden deceleration or steering. Therefore, the LSTM network is designed and trained to realize trajectories prediction of surrounding vehicles based on the highD dataset.

Fig. 2 shows the prediction process of LSTM. The input variable is the historical lateral and longitudinal velocities, and the output is a velocity sequence of the prediction horizon. The LSTM has two main parts: the memory cell which is used to summarize the historical inputs and store the information and the gating mechanism which is used to control the related gates for outputting state and updating memory information. The left part of Fig. 2 shows the velocity-prediction process with LSTM, including the input layer, LSTM layer, fully connected layer, and output layer. For example, with a prediction horizon ($N_p = 20$) and a sampling time ($T_s = 0.05$ s), the prediction results at different times are shown in the right part of Fig. 2.

In Table I, the equations related to the memory cell and the gating mechanism are described, and the network structure used in this article is depicted as well, where \mathbf{W}_{FC} denotes the weights of fully connected layer, σ denotes the sigmoid

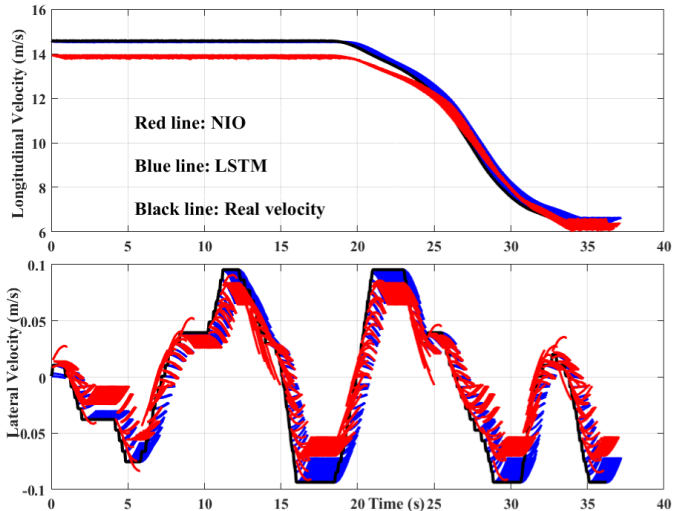


Fig. 3. Scenario of the leading car sudden deceleration.

function [40], \tanh denotes the tangent function, $\mathbf{W}_{x,i}$, $\mathbf{W}_{x,f}$, $\mathbf{W}_{x,o}$, $\mathbf{W}_{g,i}$, $\mathbf{W}_{h,i}$, $\mathbf{W}_{h,f}$, $\mathbf{W}_{h,o}$, and $\mathbf{W}_{h,i}$ represent the linear transformation matrices, b_i , b_f , b_o , and b_g denote the bias vectors, i_t , f_t , and o_t denote gate vectors, and c_t , h_t , and y_t denote the cell memory state vector and the state output vector.

The NIO network prediction algorithm is used to compare with the proposed method of LSTM in this section. Since the NIO network is a basic algorithm for solving nonlinear time series problems, it can also be used to predict the trajectory of surrounding vehicles. By giving the past values of obstacle state $x(t)$, a certain number of hidden layers are used to process the input data $x(t)$ to obtain the trajectory of the prediction horizon.

Fig. 3 shows the velocity prediction for a sudden deceleration driving scenario. The black line denotes the real velocity, and the red and the blue lines represent the velocities predicted by the NIO method and LSTM method, respectively. It shows that both the NIO and the LSTM have predicted the deceleration feature by presenting the decelerating tendency around the time of 19 s in the prediction process. However, the error between the velocities predicted by NIO and the real velocities is larger than that of LSTM, and the curve has many burrs, indicating that the prediction algorithm has certain uncertainty.

Fig. 4 shows the prediction results for a sudden lane-change driving scenario, including the lateral and longitudinal velocities. It shows that the lateral velocity presents a lane-change tendency around the time of 0 s. The blue and red lines show that the lane-change feature has been learned by both the LSTM and NIO predictors. The root-mean-squared error (RMSE) between real velocity and predictive velocity under different prediction algorithms is shown in Table II. It is obvious that the LSTM method has a smaller RMSE than the NIO method in all of the test prediction horizons, which indicates that the LSTM predictor has a higher accuracy. Besides, the results show that with the enlarge of the prediction horizon, the overall prediction precise will decrease, e.g., the RMSE is 0.04 with $N_p = 4$ versus 0.81 with $N_p = 30$ for LSTM.

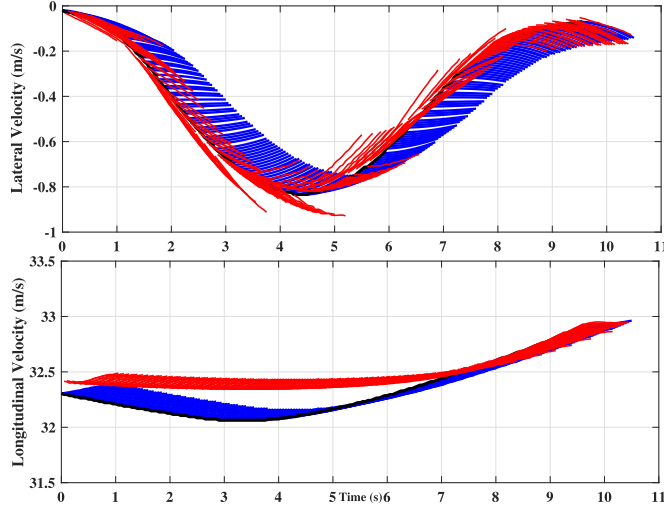


Fig. 4. Scenario of the leading car sudden steering.

IV. RISK ASSESSMENT AND MITIGATION IN PATH PLANNING WITH LSTM PREDICTION

1) *Risk Assessment Index*: The risk assessment index (RAI) is related to the traffic participant on road, which can be categorized as noncrossable participants (e.g., other vehicles and pedestrians), crossable participants (e.g., water bottles and small boxes), and road boundaries. The RAI can be defined as

$$RAI = k_{NC} \sum_i^m RAI_{NC,i} + k_C \sum_j^n RAI_{C,j} + k_R \sum_k^q RAI_{R,k} \quad (1)$$

where k_{NC} , k_C , and k_R denote the weights of RAI related to the noncrossable traffic participants, crossable participants, and road boundary, respectively. The subscripts of i , j , and k represent the index of noncrossable traffic participants, crossable traffic participants, and road boundary, respectively. Vehicle states, the decision from the risk assessment framework, and obstacle states are then transmitted through V2V communication to the LSTM-based learning in the surrounding vehicles' trajectory prediction module. In the proposed framework, V2V is implemented on passing measured state variables, but distributed state estimation could definitely improve the performance and reliability of the required data by the prediction module of the framework in case of faults and long delays.

The RAI of noncrossable participant is calculated in

$$\left\{ \begin{array}{l} RAI_{NC,i} = k_u \frac{a_i}{s_i^{b_i}} + k_w \frac{W_0}{W} \\ s_i = \left\| \left(\frac{dX}{X_{s,i}}, \frac{dY}{Y_{s,i}} \right) \right\| \\ X_{s,i} = X_o + u T_0 + \frac{\Delta u_{a,i}^2}{2a_n} \\ Y_{s,i} = Y_o + (u \sin \theta + u_{o,i} \sin \theta) T_0 + \frac{\Delta v_{a,i}^2}{2a_n} \end{array} \right. \quad (2)$$

where a_i and b_i are the shape and intensity parameters, respectively; $\Delta u_{a,i}$ and $\Delta v_{a,i}$ represent the longitudinal and lateral

TABLE II
RMSE

Prediction Horizon	$N_p = 5$	$N_p = 10$	$N_p = 20$	$N_p = 30$
LSTM: RMSE	0.04	0.16	0.68	0.81
NIO: RMSE	0.051	0.23	0.83	1.02

approaching velocities, respectively; a_n denotes the maximum deceleration considering the comfort; θ is the heading angle toward each other; dX and dY represent the longitudinal and lateral distances between the ego vehicle and noncrossable participants, respectively; $Y_{s,i}$ and $X_{s,i}$ denote the safe lateral and longitudinal distances from the noncrossable participant, respectively; X_o and Y_o are the minimum longitudinal and lateral distances; T_0 denotes the safe time gap; u and $u_{o,i}$ are the velocities of ego vehicle and obstacles, respectively; W_0 and W are the weights of noncrossable participant and the ego vehicle, respectively; and k_u and k_w are the weights of RAI.

The RAI of crossable participant is defined as

$$\left\{ \begin{array}{l} RAI_{C,j} = a_j e^{-b_j s_j} \\ s_j = \left\| \left(\frac{dX}{X_{s,j}}, \frac{dY}{Y_{s,j}} \right) \right\| \\ X_{s,j} = X_o + u T_0 + \frac{\Delta u_{a,j}^2}{2a_n} \\ Y_{s,j} = Y_o + (u \sin \theta + u_{o,j} \sin \theta) T_0 + \frac{\Delta v_{a,j}^2}{2a_n} \end{array} \right. \quad (3)$$

where a_j and b_j are the shape and intensity parameters of crossable participant, respectively; $\Delta u_{a,j}$ and $\Delta v_{a,j}$ represent the longitudinal and lateral approaching velocities, respectively; $Y_{s,j}$ and $X_{s,j}$ denote the safe lateral and longitudinal distances from the noncrossable participant; and $u_{o,j}$ is the velocity of the crossable obstacle.

When the ego vehicle drives on the road, especially on the highway, the vehicle cannot depart the road lane marker unless a lane change is required. Meanwhile, hitting the road isolated belt is forbidden, which can cause instability or a serious car crash. Quadratic form functions are utilized here to define the RAI of the road boundary for avoiding undesirable road crossings

$$RAI_{R,k} = \begin{cases} a_k \|S_{R,k} - D_a\|, & S_{R,k} < D_a \\ 0, & S_{R,k} \geq D_a \end{cases} \quad (4)$$

where $S_{R,k}$ is the signed distance (SD) distance of the vehicle from the road boundary, D_a is the permitted distance from road boundary, index $k = r, l$ is the right or left road lane marker, and a_k represents the intensity parameter. The conclusion can be drawn that the RAI is related to the distance between the ego vehicle and the road boundary, the permitted distance from road boundary, and the intensity parameter of the road boundary.

For example, Fig. 5 shows a path planning process based on the RAI, and the higher density of black lines represents a higher risk. Obviously, the planned route (the red line) owes the lowest risk during the obstacle avoidance, which will lead the ego vehicle driving as safe as possible for collision avoidance.

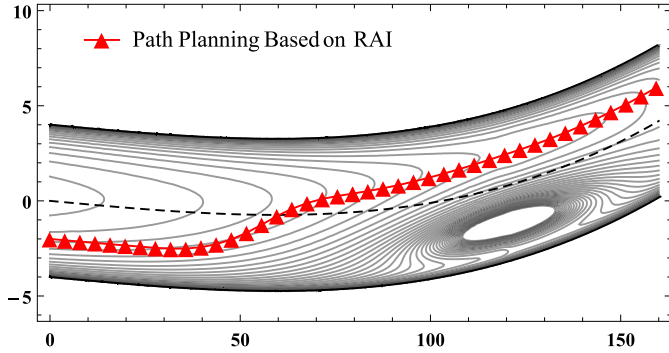


Fig. 5. Path planning based on RAI.

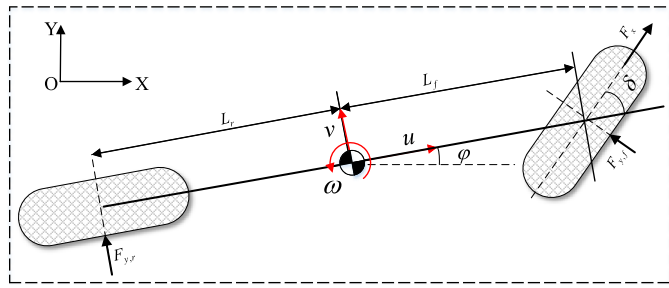


Fig. 6. Three-DOF vehicle dynamics model.

2) *Vehicle Dynamics Model*: The three-DOF vehicle dynamics model [41] is used to design the MPC controller for balancing the computation cost and the modeling accuracy. Fig. 6 shows the three-DOF model with longitudinal, lateral, and yaw dynamics variables.

The formulations for three-DOF dynamics model are presented in

$$\begin{cases} m(\dot{v}_x - \omega v_y) = F_x \cos \delta \\ m(\dot{v}_y + \omega v_x) = F_{y,r} + F_{y,f} \cos \delta \\ I_z \dot{\omega} = F_{y,f} L_f \cos \delta - F_{y,r} L_r. \end{cases} \quad (5)$$

The motion formulations [42] of the vehicle are shown in

$$\begin{cases} \dot{X} = v_x \cos \varphi - v_y \sin \varphi \\ \dot{Y} = v_x \sin \varphi + v_y \cos \varphi \end{cases} \quad (6)$$

where v_x , v_y , and ω are the longitudinal velocity, lateral velocity, and yaw rate of the vehicle, respectively; X , Y , and φ denote the longitudinal, lateral position, and the heading angle, respectively; m and F_x represent the vehicle mass and longitudinal force of the front-driving tire, respectively; $F_{y,f}$ and $F_{y,r}$ denote the lateral force of front and rear tires; and L_f , L_r , and I_z represent the front, rear wheelbase, and the vehicle inertia around vertical axis, respectively.

The lateral tire forces are calculated based on the assumption of linear tire model as

$$\begin{cases} F_{y,f} = C_f \alpha_f = C_f \left(\frac{v_y + L_f \omega}{v_x} - \delta \right) \\ F_{y,r} = C_r \alpha_r = C_r \left(\frac{v_y - L_r \omega}{v_x} \right) \end{cases} \quad (7)$$

where C_f and C_r denote the corner-stiffness values of the front and rear tires, respectively, α_f and α_r are the sideslip angle

of the front and rear tires, respectively, and δ represents the steering angle of the front tire.

The above nonlinear vehicle dynamics model is linearized and discretized with the Taylor polynomial and Euler method, respectively. The linearized and discretized model can be described as

$$\begin{cases} x(k) = [v_x(k), v_y(k), \varphi(k), \omega(k), X(k), Y(k)]^T \\ u(k) = [F_x(k), \delta(k)]^T \\ x(k+1) = \mathbf{A}_d x(k) + \mathbf{B}_d u(k) \\ y(k) = \mathbf{C}_d x(k) \\ \mathbf{A}_d \in \mathbb{R}^{N_s \times N_s}, \quad \mathbf{B}_d \in \mathbb{R}^{N_s \times N_u}, \quad \mathbf{C}_d \in \mathbb{R}^{N_y \times N_s} \end{cases} \quad (8)$$

where \mathbf{A}_d , \mathbf{B}_d , and \mathbf{C}_d are the discrete matrices, $x(k)$ and $u(k)$ denote the current discrete state variables and control variables, respectively, and N_s , N_u , and N_y represent the number of state variables, control variables, and output variables, respectively.

3) *Multiconstraint*: The road regulations, control variables, and output variables' constraints are considered in MPC controller. The constraint of road regulations includes the velocity limitation as

$$0 \leq v_x \leq v_x^{\max}$$

where v_x^{\max} represents the maximum vehicle velocity.

The constraints of control variables include the boundary limitations and the increment limitations as

$$\begin{bmatrix} F_{x,\max} \\ \delta_{\max} \\ \Delta F_{x,\max} \\ \Delta \delta_{\max} \end{bmatrix} \leq \begin{bmatrix} F_x \\ \delta \\ \Delta F_x \\ \Delta \delta \end{bmatrix} \leq \begin{bmatrix} F_{x,\min} \\ \delta_{\min} \\ \Delta F_{x,\min} \\ \Delta \delta_{\min} \end{bmatrix}.$$

The lateral and longitudinal tire forces are limited within the friction ellipse

$$\left(\frac{F_x}{F_{x,\max}} \right)^2 + \left(\frac{F_y}{F_{y,\max}} \right)^2 \leq \mu^2$$

where $F_{x,\max}$ is the maximum tire longitudinal force, $F_{y,\max}$ is the maximum lateral tire force, and μ is the road adhesion coefficient.

Meanwhile, the friction ellipse is varying with the vertical load transfer. Considering the longitudinal load transfer, the vertical load of the rear and front tire is described as

$$\begin{cases} F_{z,f} = \frac{mgL_r}{L_f + L_r} - \frac{F_x h}{L_f + L_r} \\ F_{z,r} = \frac{mgL_f}{L_f + L_r} + \frac{F_x h}{L_f + L_r} \end{cases} \quad (9)$$

where g and h denote the gravity acceleration and the centroid height, respectively.

The ellipse constraints of tire force are regulated as

$$\begin{cases} \left(\frac{F_x}{F_{x,\max}} \right)^2 + \left(\frac{F_{y,f}}{F_{y,f}^{\max}} \cdot \frac{\omega L_r}{\omega L_r - F_x h} \right)^2 \leq \mu^2 \\ \left(\frac{F_x}{F_{x,\max}} \right)^2 + \left(\frac{F_{y,r}}{F_{y,r}^{\max}} \cdot \frac{\omega L_f}{\omega L_f + F_x h} \right)^2 \leq \mu^2. \end{cases}$$

Since the quadratic programming (QP)-based MPC requires the linear constraint functions and the convex feasible set, the hexagon is used to approximate the friction ellipse [43].

4) *LSTM-MPC*: The MPC cost function is formulated with the RAI term, the trajectory tracking term, and the slack variables that are designed for expanding the feasible region. The trajectory tracking term can be transferred into the standard quadratic formulation as

$$\begin{aligned} \mathbf{J}_1 &= \|\mathbf{Y}_{\text{pre}} - \mathbf{Y}_{\text{ref}}\|_{\tilde{\mathbf{Q}}}^2 + \|\mathbf{U}\|_{\tilde{\mathbf{R}}}^2 \\ &= \frac{1}{2} \mathbf{U}^T \underbrace{2(\mathbf{G}_m^T \tilde{\mathbf{Q}} \mathbf{G}_m + \tilde{\mathbf{R}})}_{\mathbf{H}_1} \mathbf{U} + \underbrace{2(\mathbf{E}_m^T \tilde{\mathbf{Q}} \mathbf{G}_m)}_{\mathbf{g}_1^T} \mathbf{U} + \mathbf{E}_m^T \tilde{\mathbf{Q}} \mathbf{E}_m \end{aligned} \quad (10)$$

where \mathbf{H}_1 and \mathbf{g}_1 represent the Hessian and gradient matrices of the cost term \mathbf{J}_1 , respectively; \otimes is the Kronecker product; \mathbf{E}_m and \mathbf{G}_m are used for simplicity; $\tilde{\mathbf{A}}$ and $\tilde{\mathbf{B}}$ are prediction matrices in the prediction horizon (N_p); and \mathbf{Q} and \mathbf{R} are weights matrices of the state variable and the control variable, respectively

$$\begin{aligned} \mathbf{E}_m &= \tilde{\mathbf{A}}x(k) - \mathbf{Y}_{\text{ref}} \\ \mathbf{G}_m &= \tilde{\mathbf{B}} \\ \tilde{\mathbf{Q}} &= \mathbf{I}^{(N_p+1) \times (N_p+1)} \otimes \mathbf{Q}^{N_y \times N_y} \\ \tilde{\mathbf{R}} &= \mathbf{I}^{N_c \times N_c} \otimes \mathbf{R}^{N_u \times N_u} \\ \tilde{\mathbf{A}} &= \left[\mathbf{C}_d \mathbf{A}_d, \mathbf{C}_d \mathbf{A}_d^2, \dots, \mathbf{C}_d \mathbf{A}_d^{N_p} \right]^T \\ \tilde{\mathbf{B}} &= \begin{bmatrix} \mathbf{C}_d \mathbf{B}_d & 0 & \dots & 0 \\ \mathbf{C}_d \mathbf{A}_d \mathbf{B}_d & \mathbf{C}_d \mathbf{B}_d & \dots & 0 \\ \vdots & \vdots & \ddots & \vdots \\ \mathbf{C}_d \mathbf{A}_d^{S_1} \mathbf{B}_d & \mathbf{C}_d \mathbf{A}_d^{S_2} \mathbf{B}_d & \dots & \mathbf{C}_d \mathbf{A}_d^{S_N} \mathbf{B}_d \end{bmatrix} \\ S_1 &= N_p - 1, \quad S_2 = N_p - 2, \quad S_N = N_p - N_c - 2. \end{aligned}$$

The longitudinal and lateral distances can be calculated as

$$\begin{cases} s_x^k = X(k) - X_{\text{obs}}(k) \\ s_y^k = Y(k) - Y_{\text{obs}}(k) \end{cases} \quad (11)$$

where s_i^k ($i = x, y$) denotes the longitudinal and lateral distances from the ego vehicle to the obstacle at the time of k and $(X(k), Y(k))$ and $(X_{\text{obs}}(k), Y_{\text{obs}}(k))$ are the current positions of ego vehicle and obstacle vehicle, respectively. Then, the values of (1)–(4) are obtained based on the distances between the ego vehicle and the obstacles of (11). The RAI function is a nonlinear and nonconvex function, which cannot be solved directly by the traditional QP solvers. Usually, this kind of problem can be solved with the sequential QP (SQP) method, in which the main idea is to approximate the primal nonlinear and nonconvex problem to a series of convex subproblems. The primal RAI function is approximated to the quadratic formulation based on the Taylor approximation method

$$\begin{cases} \chi_i(k) = \begin{bmatrix} s_{x,i}^k & s_{y,i}^k \end{bmatrix}^T, \quad i = \text{NC, C, R} \\ \hat{R}_i(\chi(k)) \approx \frac{1}{2} \chi_i(k)^T \mathbf{H}_{2,i} \chi_i(k) + \mathbf{g}_{2,i}^T \chi_i(k) \end{cases} \quad (12)$$

where $i = \text{NC, C, R}$ denotes the noncrossable, crossable, and road obstacles, respectively; $\chi_i(k)$ is the longitudinal and lateral distances from the ego vehicle to the i th obstacle; $\hat{R}_i(\chi(k))$ is the approximate quadratic formulation of RAI_i

defined in (1); and the equivalent gradient and Hessian matrices are as

$$\mathbf{g}_{2,i}^T = \nabla \text{RAI}_i(\chi_i(k)) = \begin{bmatrix} \frac{\partial \text{RAI}_i}{\partial s_{x,i}^k} & \frac{\partial \text{RAI}_i}{\partial s_{y,i}^k} \end{bmatrix}$$

and

$$\mathbf{H}_{2,i} = \nabla^2 \text{RAI}_i(\chi_i(k)) = \begin{bmatrix} \frac{\partial^2 \text{RAI}_i}{\partial s_{x,i}^k \partial s_{x,i}^k} & \frac{\partial^2 \text{RAI}_i}{\partial s_{x,i}^k \partial s_{y,i}^k} \\ \frac{\partial^2 \text{RAI}_i}{\partial s_{y,i}^k \partial s_{x,i}^k} & \frac{\partial^2 \text{RAI}_i}{\partial s_{y,i}^k \partial s_{y,i}^k} \end{bmatrix}$$

respectively.

The detailed convex process can be found in [44]. Finally, the optimization problem can be described as

$$\begin{aligned} \min J &= \min_{u, \varepsilon} \sum_{k=1}^{N_p} J_1(k) + \text{RAI}_t^{t+k} + \|\varepsilon_k\|_{\mathbf{P}}^2 \\ \text{s.t. } (k &= 1, \dots, N_p) \\ x^{t+k, t} &= \mathbf{A}_d x_t^{t+k-1} + \mathbf{B}_d u_t^{t+k-1} \\ y_t^{t+k} &= \mathbf{C}_d x_t^{t+k} + \mathbf{D}_d u_t^{t+k} \\ y_{s,t}^{t+k} &= \mathbf{C}_s x_t^{t+k} + \mathbf{D}_s u_t^{t+k} \\ y_{s,t}^{t+k} &\leq y_{s,\text{max},t}^{t+k} + \varepsilon_k, \quad \varepsilon_k \geq 0 \\ u_{\min} &< u_t^{t+k-1} < u_{\max} \\ \Delta u_{\min} &< u_t^{t+k} - u_t^{t+k-1} < \Delta u_{\max} \\ x_t^t &= x(t), \quad u_t^{t-1} = u(t-1) \end{aligned} \quad (13)$$

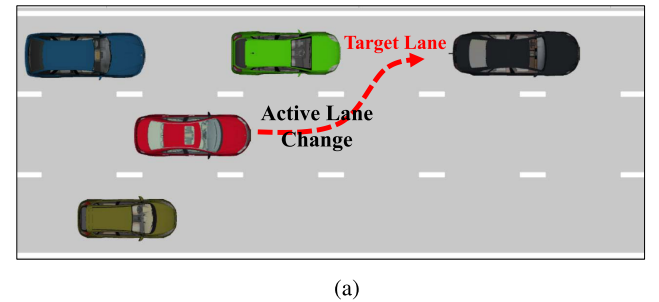
where $t + k$ represents the predicted value at k steps ahead of t . ε_k denotes the slack variables vector at k steps ahead, which represents the penalty of soft constraints on tire forces. \mathbf{C}_d and \mathbf{D}_d denote the output and feedforward matrices, $y_{s,t}$ represent the linearized constraints variables, and \mathbf{C}_s and \mathbf{D}_s denote the output and feedforward matrices of the constraint variables. The problem is, however, nonlinear and nonconvex since the term of RAI is nonlinear and nonconvex. Therefore, its solution is time-consuming. Here, it is converted into its approximated quadratic convex problem to reduce the calculation time. For brevity, the detail of the convex process is not shown here. After the convex process, the optimal control problem is a convex quadratic optimization problem. The problem is similar to a corresponding nonlinear problem solved by SQP in one sequence. The optimal problem is solved by an open-source solver qpOASES [45], [46].

V. SIMULATION RESULTS AND ANALYSIS

Two driving scenarios are constructed based on the highD dataset for validation and evaluation. The proposed LSTM-MPC is compared to the MPC with constant-velocity prediction and the NIO network predictor. The driving safety and efficiency are compared based on the RAI and the collision-avoidance velocity during path planning.

A. Scenario I

The ego vehicle is driving along Lane-2 at the beginning, and the target lane changes from Lane-2 to Lane-3 after a few miles driving. Meanwhile, there are three obstacle vehicles



(a)

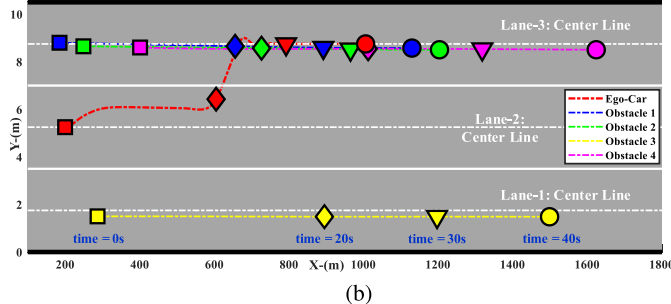


Fig. 7. (a) Scenario I: an active lane-change driving scenario. (b) Trajectories of ego vehicle and surrounding vehicles in scenario I.

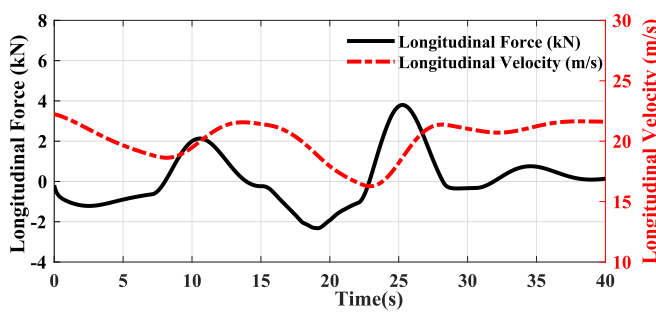


Fig. 8. Longitudinal force and longitudinal velocity of ego vehicle in scenario I.

near to the ego vehicle in Lane-3, as shown in Fig. 7(a). The ego vehicle needs to complete the lane changing without collision.

Fig. 7(b) shows the trajectories of ego vehicle and obstacle vehicles. The different shapes represent the time series and the different colors denote the different vehicles. For example, the red color denotes the ego vehicle and the square shape, the diamond shape, the lower triangle, and the circle represent position information of the ego vehicle at the time of 0, 20, 30, and 40 s, respectively.

Meanwhile, the lane-change process can be summarized in three steps based on the trajectory of the ego vehicle in Fig. 7(b). First, the ego vehicle deviates a little distance from the centerline toward the left lane boundary preparing for lane changing. Second, after the surrounding vehicles passed, the ego vehicle crosses the left lane boundary for completing the lane changing. Finally, the ego vehicle adjusts its lateral position and velocity for lane keeping in the new target lane (Lane-3).

Fig. 8 shows the vary of longitudinal tire force and velocity for ego vehicle during the active lane change in scenario I. It shows the longitudinal velocity will be adjusted for reducing

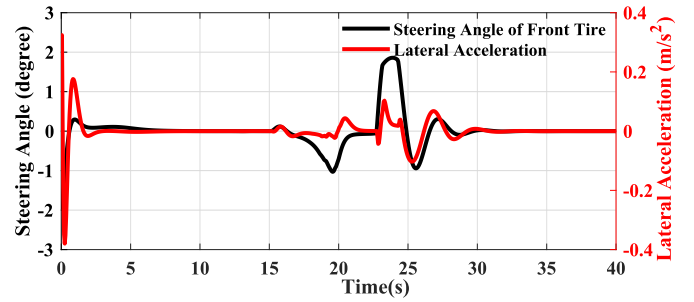


Fig. 9. Steering angle and lateral acceleration of ego vehicle in the scenario I.

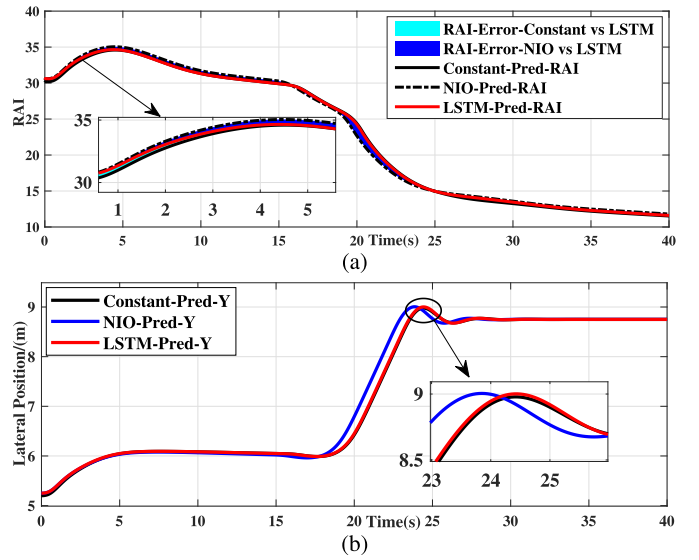


Fig. 10. Comparisons of the LSTM velocity-prediction method with NIO velocity-prediction method and the constant-velocity assumption method in scenario I: (a) RAI. (b) Lateral position.

the RAI during the lane-change process, and the longitudinal tire force is within the tire force limitation shown in the Nomenclature of [38]. Meanwhile, Fig. 9 shows the steering angle and the lateral acceleration during the lane-change process in scenario I. It shows that the ego vehicle starts with a small left steering angle preparing for lane changing at 0 s and then takes lane change from 23 to 30 s after the surrounding vehicles passed. Meanwhile, the ego vehicle will optimize the trajectory to improve the safety in real-time, e.g., at time of 20 s, the ego vehicle steers to right for reducing the RAI while the obstacle vehicles approaching.

The comparisons of lateral position and RAI among the LSTM-MPC, NIO-MPC, and a conventional MPC are shown in Fig. 10. The results in Fig. 10(a) shows that path planning with LSTM-MPC owes the lowest RAI than the other two methods, and the NIO-MPC method has the slightly highest RAI with a maximum error of 0.5 at time of 4 s. The lateral positions of LSTM-MPC and traditional MPC are compared in Fig. 10(b) during lane changing. However, because of higher prediction uncertainty, the lateral position of NIO-MPC deviated from the actual scenario to some extent.

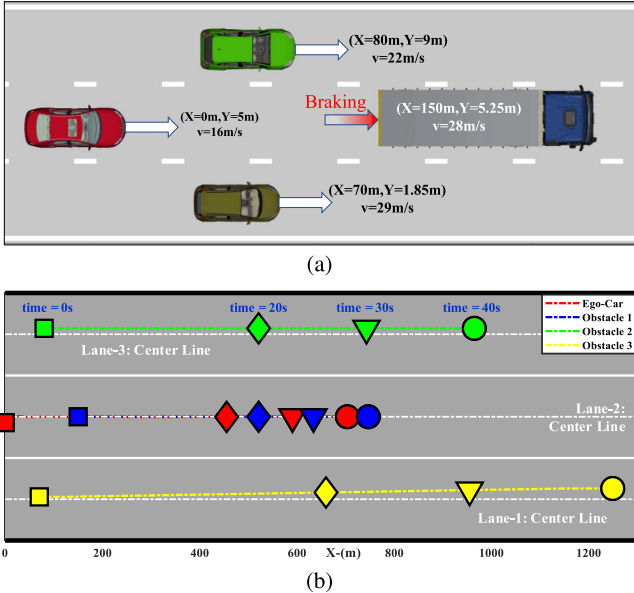


Fig. 11. (a) Scenario II: emergency braking driving scenario. (b) Trajectories of ego vehicle and obstacles in scenario II.

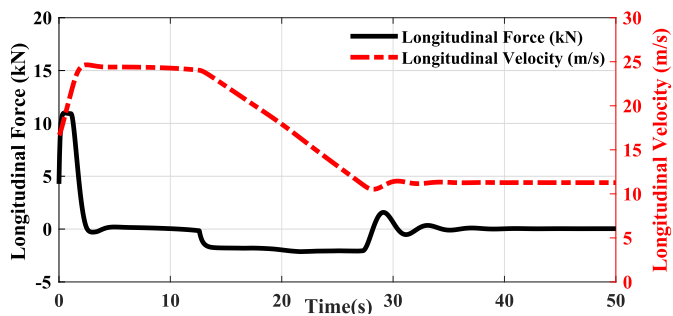


Fig. 12. Longitudinal force and longitudinal velocity of ego vehicle in scenario II.

B. Scenario II

Scenario II is constructed to simulate a sudden deceleration situation for evaluation. It depicts that the ego vehicle is following a leading truck in Lane-2 at the beginning, and then, the truck sudden decelerates to a low speed after a few miles driving, as shown in Fig. 11(a).

The trajectory of the ego vehicle is shown in Fig. 11(b) during the sudden deceleration of a leading truck in scenario II. The blue and red colors represent the truck and ego vehicle, respectively, and the truck has a sudden deceleration around the time of 15 s. It shows that the ego vehicle will also decelerate with the leading truck to keep a safe distance for lane keeping.

The longitudinal tire force and velocity of the ego vehicle are shown in Fig. 12 during the decelerating of the leading truck in scenario II. It shows that the ego vehicle will accelerate to the target velocity (25 m/s) when there is no sudden deceleration, and the ego vehicle will decelerate to the same velocity as the leading truck (12 m/s) with a safe distance when the sudden deceleration happens. The steering angle and lateral acceleration of the ego vehicle are shown in Fig. 13 during the sudden deceleration process. It shows that the initial lateral

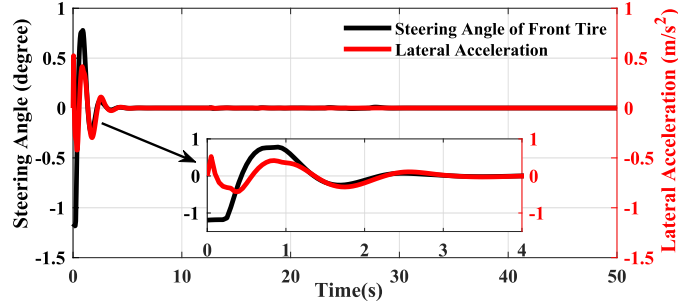


Fig. 13. Steering angle and lateral acceleration of ego vehicle in scenario II.

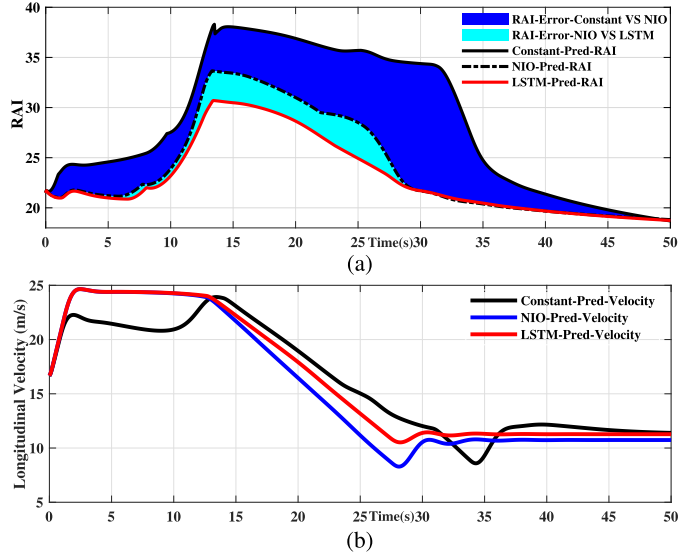


Fig. 14. Comparisons of the LSTM velocity-prediction method with NIO velocity-prediction method and the constant-velocity assumption method in scenario II: (a) RAI comparison. (b) Longitudinal velocity comparison.

error will be eliminated in time by steering control with a limitation of maximum lateral acceleration.

Fig. 14 shows the RAIs of the three approaches. It indicates that the ego vehicle will decelerate with the leading vehicle for collision avoidance in all methods. With the LSTM and NIO method, the ego vehicle will decelerate in advance, and the RAI is improved comparing to the constant method. However, due to a lower prediction precise of NIO, this results in an unnecessary bigger deceleration than the other two methods. In addition, the RAI of LSTM-MPC is the lowest among the three methods, which indicates that the ego vehicle has a higher safe level using the LSTM-MPC for path planning and path tracking. It also indicates that the ego vehicle can drive with a lower risk and shorter decelerating time with LSTM-MPC by considering the velocities of surrounding vehicles during autonomous driving.

VI. CONCLUSION

This article proposed a path planning approach based on risk assessment and mitigation. An LSTM network is trained and used to predict the trajectories of surrounding vehicles based on the highD dataset. The velocities of surrounding vehicles

are based to assess the risk to assist improving the driving safety of AVs by introducing the index of RAI. Two typical scenarios are constructed for validation and evaluation based on the real data from the highD dataset, including an active lane-change scenario with constant-speed surrounding vehicles and a lane-keeping scenario with a sudden deceleration of the leading vehicle.

The proposed method is compared with an NIO-MPC and conventional MPC methods in these two driving scenarios. The comparisons of RAI show that the ego vehicle with LSTM-MPC always has the lowest RAI (the highest safety) during the autonomous driving both in the active lane-change and the deceleration scenarios. Meanwhile, the comparisons of RAI between the proposed method and the NIO method also illustrate that the higher prediction precise for the surrounding vehicles, the safer the ego vehicle is during path planning and tracking. All the simulation results support the conclusion that the ego vehicle with LSTM-MPC occupies a smaller RAI and higher driving efficiency than that of the Const-MPC and NIO network predictor.

In future, a series of experiments with the proposed algorithm will be implemented in real vehicle, and the relevant tests about safety of the intended functionality will be proceeded as well for stability and robustness improvements.

REFERENCES

- [1] D. Bissell, "Automation interrupted: How autonomous vehicle accidents transform the material politics of automation," *Political Geography*, vol. 65, pp. 57–66, Jul. 2018.
- [2] P. O. Forum, "Autonomous vehicles: No driver... no regulation?" *Science*, vol. 361, no. 6397, pp. 36–37, Jul. 2018.
- [3] B. Vlasic and N. E. Boudette, "Self-driving tesla was involved in fatal crash, US says," *New York Times*, vol. 302016, Jun. 2016.
- [4] J. Cui, L. S. Liew, G. Sabaliauskaitė, and F. Zhou, "A review on safety failures, security attacks, and available countermeasures for autonomous vehicles," *Ad Hoc Netw.*, vol. 90, Jul. 2019, Art. no. 101823.
- [5] H. Gao *et al.*, "Situational assessment for intelligent vehicles based on stochastic model and Gaussian distributions in typical traffic scenarios," *IEEE Trans. Syst., Man, Cybern. Syst.*, early access, Sep. 18, 2020, doi: 10.1109/TSMC.2020.3019512.
- [6] H. Wang, Y. Huang, A. Khajepour, D. Cao, and C. Lv, "Ethical decision-making platform in autonomous vehicles with lexicographic optimization based model predictive controller," *IEEE Trans. Veh. Technol.*, vol. 69, no. 8, pp. 8164–8175, Aug. 2020.
- [7] Y. Huang, H. Wang, A. Khajepour, H. Ding, K. Yuan, and Y. Qin, "A novel local motion planning framework for autonomous vehicles based on resistance network and model predictive control," *IEEE Trans. Veh. Technol.*, vol. 69, no. 1, pp. 55–66, Jan. 2020.
- [8] J. Ziegler and M. Werling, "Navigating car-like robots in unstructured environments using an obstacle sensitive cost function," in *Proc. IEEE Intell. Vehicles Symp.*, Jun. 2008, pp. 787–791.
- [9] J. Young Hwang, J. Song Kim, S. Seok Lim, and K. Ho Park, "A fast path planning by path graph optimization," *IEEE Trans. Syst., Man, Cybern., A, Syst. Humans*, vol. 33, no. 1, pp. 121–128, Jan. 2003.
- [10] Y. Kuwata, S. Karaman, J. Teo, E. Frazzoli, J. P. How, and G. Fiore, "Real-time motion planning with applications to autonomous urban driving," *IEEE Trans. Control Syst. Technol.*, vol. 17, no. 5, pp. 1105–1118, Sep. 2009.
- [11] B. Lu *et al.*, "Adaptive potential field-based path planning for complex autonomous driving scenarios," *IEEE Access*, vol. 8, pp. 225294–225305, Dec. 2020.
- [12] B. Lu *et al.*, "Hybrid path planning combining potential field with sigmoid curve for autonomous driving," *Sensors*, vol. 20, no. 24, p. 7197, Dec. 2020.
- [13] B. Kim and J. Pineau, "Socially adaptive path planning in human environments using inverse reinforcement learning," *Int. J. Social Robot.*, vol. 8, no. 1, pp. 51–66, Jun. 2015.
- [14] P. M. Kebria, A. Khosravi, S. M. Salaken, and S. Nahavandi, "Deep imitation learning for autonomous vehicles based on convolutional neural networks," *IEEE/CAA J. Automatica Sinica*, vol. 7, no. 1, pp. 82–95, Jan. 2020.
- [15] J. Li, Q. Li, N. Chen, and Y. Wang, "Indoor pedestrian trajectory detection with LSTM network," in *Proc. 7th IEEE Int. Conf. Comput. Sci. Eng. (CSE) IEEE Int. Conf. Embedded Ubiquitous Comput. (EUC)*, Jul. 2017, pp. 651–654.
- [16] X. Na and D. J. Cole, "Modelling of a human driver's interaction with vehicle automated steering using cooperative game theory," *IEEE/CAA J. Automatica Sinica*, vol. 6, no. 5, pp. 1095–1107, Sep. 2019.
- [17] M. Schreier, V. Willert, and J. Adamy, "An integrated approach to maneuver-based trajectory prediction and criticality assessment in arbitrary road environments," *IEEE Trans. Intell. Transp. Syst.*, vol. 17, no. 10, pp. 2751–2766, Oct. 2016.
- [18] S. Funfgeld, M. Holzapfel, M. Frey, and F. Gauterin, "Stochastic forecasting of vehicle dynamics using sequential Monte Carlo simulation," *IEEE Trans. Intell. Vehicles*, vol. 2, no. 2, pp. 111–122, Jun. 2017.
- [19] Y. Li, H. He, and J. Peng, "An adaptive online prediction method with variable prediction horizon for future driving cycle of the vehicle," *IEEE Access*, vol. 6, pp. 33062–33075, May 2018.
- [20] J. Guo, H. He, and C. Sun, "ARIMA-based road gradient and vehicle velocity prediction for hybrid electric vehicle energy management," *IEEE Trans. Veh. Technol.*, vol. 68, no. 6, pp. 5309–5320, Jun. 2019.
- [21] H. Tan, Y. Wu, B. Shen, P. J. Jin, and B. Ran, "Short-term traffic prediction based on dynamic tensor completion," *IEEE Trans. Intell. Transp. Syst.*, vol. 17, no. 8, pp. 2123–2133, Aug. 2016.
- [22] D. Lee, C. Liu, Y.-W. Liao, and J. K. Hedrick, "Parallel interacting multiple model-based human motion prediction for motion planning of companion robots," *IEEE Trans. Autom. Sci. Eng.*, vol. 14, no. 1, pp. 52–61, Jan. 2017.
- [23] G. Xie, H. Gao, L. Qian, B. Huang, K. Li, and J. Wang, "Vehicle trajectory prediction by integrating physics- and maneuver-based approaches using interactive multiple models," *IEEE Trans. Ind. Electron.*, vol. 65, no. 7, pp. 5999–6008, Jul. 2018.
- [24] V. Fox, J. Hightower, L. Liao, D. Schulz, and G. Borriello, "Bayesian filtering for location estimation," *IEEE Pervas. Comput.*, vol. 2, no. 3, pp. 24–33, Jul. 2003.
- [25] R. Quintero Minguez, I. Parra Alonso, D. Fernandez-Llorca, and M. A. Sotelo, "Pedestrian path, pose, and intention prediction through Gaussian process dynamical models and pedestrian activity recognition," *IEEE Trans. Intell. Transp. Syst.*, vol. 20, no. 5, pp. 1803–1814, May 2019.
- [26] S. Lefevre, A. Carvalho, and F. Borrelli, "A learning-based framework for velocity control in autonomous driving," *IEEE Trans. Autom. Sci. Eng.*, vol. 13, no. 1, pp. 32–42, Jan. 2016.
- [27] P. Bansal and K. M. Kockelman, "Forecasting Americans' long-term adoption of connected and autonomous vehicle technologies," *Transp. Res. A: Policy Pract.*, vol. 95, pp. 49–63, Jan. 2017.
- [28] Y. Li, R. Yu, C. Shahabi, and Y. Liu, "Diffusion convolutional recurrent neural network: Data-driven traffic forecasting," 2017, *arXiv:1707.01926*. [Online]. Available: <http://arxiv.org/abs/1707.01926>
- [29] S. Hochreiter, "Long short-term memory," *Neural Comput.*, vol. 1780, pp. 1735–1780, Nov. 1997.
- [30] N. Deo and M. M. Trivedi, "Multi-modal trajectory prediction of surrounding vehicles with maneuver based LSTMs," in *Proc. IEEE Intell. Vehicles Symp. (IV)*, Jun. 2018, pp. 1179–1184.
- [31] H. Gao *et al.*, "Trajectory prediction of cyclist based on dynamic Bayesian network and long short-term memory model at unsignalized intersections," *Sci. China, Inf. Sci.*, vol. 64, no. 7, pp. 172207:1–172207:13, 2021.
- [32] X. Ma, Z. Tao, Y. Wang, H. Yu, and Y. Wang, "Long short-term memory neural network for traffic speed prediction using remote microwave sensor data," *Transp. Res. C, Emerg. Technol.*, vol. 54, pp. 187–197, May 2015.
- [33] T. Guo, Z. Xu, X. Yao, H. Chen, K. Aberer, and K. Funaya, "Robust online time series prediction with recurrent neural networks," in *Proc. IEEE Int. Conf. Data Sci. Adv. Analytics (DSAA)*, Oct. 2016, pp. 816–825.
- [34] V. Turri, B. Besseling, and K. H. Johansson, "Cooperative look-ahead control for fuel-efficient and safe heavy-duty vehicle platooning," *IEEE Trans. Control Syst. Technol.*, vol. 25, no. 1, pp. 12–28, Jan. 2017.
- [35] M. Pirani *et al.*, "Cooperative vehicle speed fault diagnosis and correction," *IEEE Trans. Intell. Transp. Syst.*, vol. 20, no. 2, pp. 783–789, Feb. 2019.

- [36] S. Ucar, S. C. Ergen, and O. Ozkasap, "IEEE 802.11p and visible light hybrid communication based secure autonomous platoon," *IEEE Trans. Veh. Technol.*, vol. 67, no. 9, pp. 8667–8681, Sep. 2018.
- [37] S. Darbha, S. Konduri, and P. R. Pagilla, "Benefits of V2 V communication for autonomous and connected vehicles," *IEEE Trans. Intell. Transp. Syst.*, vol. 20, no. 5, pp. 1954–1963, May 2019.
- [38] R. Krajewski, J. Bock, L. Kloeker, and L. Eckstein, "The highD dataset: A drone dataset of naturalistic vehicle trajectories on German highways for validation of highly automated driving systems," in *Proc. 21st Int. Conf. Intell. Transp. Syst. (ITSC)*, Nov. 2018, pp. 2118–2125.
- [39] L. Chen, X. Hu, W. Tian, H. Wang, D. Cao, and F.-Y. Wang, "Parallel planning: A new motion planning framework for autonomous driving," *IEEE/CAA J. Automatica Sinica*, vol. 6, no. 1, pp. 236–246, Jan. 2019.
- [40] G. Li, Y. Yang, and X. Qu, "Deep learning approaches on pedestrian detection in hazy weather," *IEEE Trans. Ind. Electron.*, vol. 67, no. 10, pp. 8889–8899, Oct. 2020, doi: 10.1109/TIE.2019.2945295.
- [41] H. Guo *et al.*, "Hazard-evaluation-oriented moving horizon parallel steering control for driver-automation collaboration during automated driving," *IEEE/CAA J. Automatica Sinica*, vol. 5, no. 6, pp. 1062–1073, Nov. 2018.
- [42] C. Huang, F. Naghdy, H. Du, and H. Huang, "Shared control of highly automated vehicles using steer-by-wire systems," *IEEE/CAA J. Automatica Sinica*, vol. 6, no. 2, pp. 410–423, Mar. 2019.
- [43] H. Wang, Y. Huang, A. Khajepour, Y. Zhang, Y. Rasekipour, and D. Cao, "Crash mitigation in motion planning for autonomous vehicles," *IEEE Trans. Intell. Transp. Syst.*, vol. 20, no. 9, pp. 3313–3323, Sep. 2019.
- [44] Y. Rasekipour, A. Khajepour, S.-K. Chen, and B. Litkouhi, "A potential field-based model predictive path-planning controller for autonomous road vehicles," *IEEE Trans. Intell. Transp. Syst.*, vol. 18, no. 5, pp. 1255–1267, May 2017.
- [45] H. J. Ferreau, C. Kirches, A. Potschka, H. G. Bock, and M. Diehl, "qpOASES: A parametric active-set algorithm for quadratic programming," *Math. Program. Comput.*, vol. 6, no. 4, pp. 327–363, Apr. 2014.
- [46] J. Ni, J. Hu, and C. Xiang, "Envelope control for four-wheel independently actuated autonomous ground vehicle through AFS/DYC integrated control," *IEEE Trans. Veh. Technol.*, vol. 66, no. 11, pp. 9712–9726, Nov. 2017.



Hong Wang received the Ph.D. degree from the Beijing Institute of Technology, Beijing, China, in 2015.

From 2015 to 2019, she worked with the University of Waterloo, Waterloo, ON, Canada, as a Post-Doctoral Researcher. She is currently an Associate Research Professor with the School of Vehicle and Mobility, Tsinghua University, Beijing. Her research focuses on the path planning control and ethical decision-making for autonomous vehicles and component sizing; modeling of hybrid powertrains and power management control strategies design for hybrid electric vehicles; and intelligent control theory and application.



Bing Lu received the M.S. degree from the School of Mechanical and Vehicular Engineering, Beijing Institute of Technology, Beijing, China, in 2015, where he is currently pursuing the Ph.D. degree in mechanical engineering with the National Engineering Laboratory for Electric Vehicles.

His current research interests include dynamics modeling and simulation and path planning and tracking control for intelligent electrified vehicles.



Jun Li received the Ph.D. degree in vehicle engineering from Jilin University, Changchun, China, in 1989.

He is currently an Academician of the Chinese Academy of Engineering, Beijing, China, a Professor with the School of Vehicle and Mobility, Tsinghua University, Beijing, the President of the Society of Automotive Engineers of China, Beijing, and the Director of the expert committee of China Industry Innovation Alliance for the Intelligent and Connected Vehicles, Beijing. His research interests include internal combustion engines, electric drive systems, electric vehicles, intelligent vehicles, and connected vehicles.



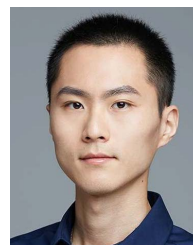
Teng Liu (Member, IEEE) received the B.S. degree in mathematics and the Ph.D. degree in automotive engineering from the Beijing Institute of Technology (BIT), Beijing, China, in 2011 and 2017, respectively. His Ph.D. dissertation, under the supervision of Prof. Fengchun Sun, was entitled Reinforcement learning-based energy management for hybrid electric vehicles.

He is currently a Post-Doctoral Fellow with the Department of Mechanical and Mechatronics Engineering, University of Waterloo, Waterloo, ON, Canada. He has more than eight years of research and working experience in new-energy vehicles and connected autonomous vehicles. His current research focuses on parallel driving, parallel reinforcement learning, automated driving, and energy management of hybrid electric vehicles. He has published more than 30 articles in these areas.



Yang Xing received the Ph.D. degree from Cranfield University, Cranfield, U.K., in 2018.

He is currently a Research Fellow with the Department of Mechanical and Aerospace Engineering, Nanyang Technological University, Singapore. His research interests include machine learning, driver behavior modeling, intelligent multiagent collaboration, and intelligent/autonomous vehicles. His work focuses on the understanding of driver behaviors using machine-learning methods and intelligent and automated vehicle design.



Chen Lv (Senior Member, IEEE) received the Ph.D. degree from Tsinghua University, Beijing, China, in 2016.

From 2014 to 2015, he was a joint Ph.D. Researcher with the EECS Department, University of California, Berkeley, CA, USA. He is currently an Assistant Professor with Nanyang Technology University, Singapore. He has authored or coauthored 40 articles. He holds 11 granted China patents. His research focuses on cyber-physical systems, hybrid systems, and advanced vehicle control and intelligence.



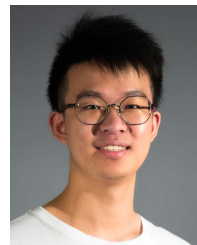
Dongpu Cao received the Ph.D. degree from Concordia University, Montreal, QC, Canada, in 2008. He is currently an Associate Professor with the University of Waterloo, Waterloo, ON, Canada. He has authored or coauthored more than 150 publications and one book. He holds one U.S. patent. His research focuses on vehicle dynamics, control, and intelligence.

Dr. Cao was a recipient of the ASME AVTT 2010 Best Paper Award and the 2012 SAE Arch T. Colwell Merit Award. He serves as an Associate Editor for IEEE TRANSACTIONS ON INTELLIGENT TRANSPORTATION SYSTEMS and so on. He also serves on the SAE International Vehicle Dynamics Standards Committee and a few ASME, SAE, IEEE technical committees.



Jingxuan Li received the bachelor's degree in vehicle engineering from the Nanjing University of Aeronautics and Astronautics, Nanjing, China, in 2018, where he is currently pursuing the degree in mechanical engineering.

He is interning at the School of Vehicle and Mobility, Tsinghua University, Beijing, China. His research focuses on vehicle system dynamics and control, by-wire system for intelligent connected vehicles, and path planning control for heavy-duty vehicles.



autonomous driving.

Jinwei Zhang received the B.S. degree in robotics engineering and electrical and computer engineering from Worcester Polytechnic Institute, Worcester, MA, USA, in June 2018. He is currently pursuing the M.S. degree in mechanical and mechatronics engineering with the University of Waterloo, Waterloo, ON, Canada, under the supervision of Prof. Dongpu Cao.

His current research focuses on the behavior analysis of lane-changing scenarios and the motion prediction of surrounding scenes applied on



Ehsan Hashemi (Member, IEEE) received the Ph.D. degree in mechanical and mechatronics engineering from the University of Waterloo, Waterloo, ON, Canada, in 2017, and the M.Sc. degree in mechanical engineering from the Amirkabir University of Technology (Tehran Polytechnic), Tehran, Iran, in 2005.

He is currently a Research Assistant Professor with the Department of Mechanical and Mechatronics Engineering, University of Waterloo. His research has resulted in several journal/conference publications (IEEE transactions and control engineering technology transfers on vehicle state estimation, fault-tolerant estimation, control theory, active vehicle safety systems, and intelligent transportation.